EFFECTS OF MELT FLOW-FIBER ORIENTATION COUPLING ON DEPOSITION IN LARGE AREA POLYMER COMPOSITE ADDITIVE MANUFACTURING

Zhaogui Wang, Douglas E. Smith
Department of Mechanical Engineering, Baylor University

Abstract

Discontinuous fiber reinforced polymer composites continue to see increasing application in large area polymer deposition additive manufacturing. Rheological behavior of molten polymer feedstock is critical in the manufacturing process where the shear thinning response of a fiber-filled polymer is significantly different from its unfilled polymer alternative. Additionally, extrudate swell directly affects the resolution of a printed part in polymer extrusion-based additive manufacturing where the presence of fibers and their associated alignment greatly affect the properties of the polymer composite melt flow. This study quantifies the effect of the fiber orientation on polymer melt flow and die swell with a custom finite element simulation. Our approach solves the fully coupled melt flow and fiber orientation tensor equations, including computation of the melt free surface in the die swell region. Computed results indicate that the magnitude of the velocity field along the direction of the flow is increased due to the presence of suspended fibers and the extrudate die swell for a fiber-filled polymer composite is much less than that of a neat polymer material. Accordingly, fiber-orientation-induced variations on flow rheology requires that the material feeding rate and printing path need to be adjusted when using filled polymers over their neat alternatives, especially for large area additive manufacturing applications.

Keywords: Large area polymer deposition additive manufacturing; Melt flow-fiber orientation coupling; Die swell; Finite element simulation

Introduction

Polymer deposition Additive Manufacturing (AM), otherwise known as Fused Filament Fabrication (FFF), is popular for its ability to create detailed structures with a relatively low-cost device. Recently, polymer deposition AM has been extended to include short fiber-filled polymer composites for producing structures of relatively large dimensions, which is referred as the Large Area Additive Manufacturing (LAAM). LAAM systems such as the custom LAAM machine at Baylor University appearing in Figure 1 typically use a single screw extruder to melt, extrude, and deposit pelletized feedstock, which ultimately yields a sufficiently high mass flow rate, facilitating the manufacturing of relatively large structures. For example, the Big Area Additive Manufacturing (BAAM) system developed by Oak Ridge National Laboratory and their collaborators is capable to create structures with large geometries up to 20-feet length $\times$ 8-feet width $\times$ 6-feet height with material deposition rates up to 100 lb/hour [1]. To date, the deposition speed of a BAAM machine is increased to over 200 times higher as compared to that of a conventional fused filament fabrication printer [2]. To improve the mechanical properties and dimensional accuracy of LAAM parts, short fiber fillers such as chopped carbon fibers are added to the polymer feedstock. Compared to neat polymers, filled thermoplastic alternatives exhibit higher material stiffness and lower coefficient of thermal expansion, which ultimately increases the industrial applicability of the LAAM technology [3].

It has been seen that the rheological behavior of polymer melt flows may vary significantly during the melt extrusion process when a second phase reinforcements is added. For example, Jain, et al. [4] found that the melt viscosity of polypropylene reduced dramatically due to the addition of a minute amount of silica nanoparticles. Nikzad, et al. [5] studied the viscosity properties of Acrylonitrile Butadiene Styrene (ABS) Iron metal-polymer composite processed through a FFF printer. Their measurements showed that the apparent viscosity increased with increasing volume fraction of iron content in the composites. Joseph, et al. [6] investigated the rheological behaviors of short sisal fiber reinforced polypropylene extrusion through a capillary rheometer. They reported that the viscosity of the composite system increased with fiber volume fraction and that the extrudate swell of the melt reduced with an increased fiber loading. In a similar study for high density polyethylene, Hideyuki, et al. [7] found that the extrudate swell of molten polymer melt reduced significantly by adding rigid fillers, and the swell ratio decreased with increased aspect ratio of the fiber reinforcements. Guo, et al. [8] conducted a rheology study for E-glass fiber-filled linear low density polyethylene both experimentally and numerically. They concluded that it is important to count the effects of rheology-fiber coupling in fitting the rheological data into numerical models. A recent work of Ajinjeru, et al. [9] specifically studied the importance of rheological properties of fiber filled thermoplastics for the BAAM system. The critical roles of the storage and loss shear moduli as well as the viscosity toward a successful printing condition were investigated and discussed. As the print volume of LAAM systems continue to increase, the rheological variation between neat polymer and their related fiber-filled composite is expected to yield much more distinguishable differences on a manufactured part.

This paper numerically characterizes the effect of fiber fillers on polymer composite melt flow through a LAAM nozzle using a finite-element-based customized MATLAB (Natick, MA, USA) code. A 2D axisymmetric shear thinning fluid flow having a short section of free extrudate is considered to simulate the polymer melt extrusion in a LAAM process. We use fiber orientation tensors to model fiber orientation [10] where isotropic rotary diffusion is assumed, and the orthotropic fitted closure [11] is employed to approximate the fourth order orientation tensor. The coupled effects of melt-flow/fiber-orientation is incorporated in the computation of the melt velocity field and the die swell of the free extrudate where nodal degrees-of-freedom are used to discretize the second order orientation tensor field. Finally, practical application of the computed results is discussed in the context of calibrating the LAAM printing parameters with a focus on the applications of fiber reinforced composites.

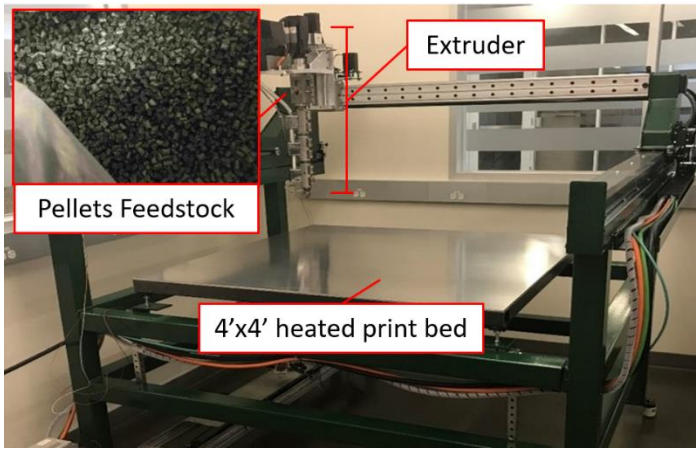

Figure 1. Baylor LAAM system composing of a Strangpresse large-scale Model 19 extruder, a 4-feet by 4-feet print-bed and associated controlling programs (not appearing in the Figure).

Methodology

A typical polymer deposition AM process includes the melting of polymer feedstock which is then extruded through a heated nozzle and deposited on a print-bed, layer-by-layer, to form a three-dimensional (3D) structure. There are numerous physical phenomena requiring in-depth investigations in order to improve the quality of a printed part (c.f. Figure 2), especially when fiber-filled polymer composites are employed. During the melt extrusion process, filled polymer melt flow exhibits a more complex rheological behavior than the unfilled neat system, as discussed in references [4-7]. The second phase reinforcements may induce significant defects in the resulting printed parts if not processed properly, and thus quantifying fiber-induced variations within the nozzle extrusion flow becomes crucial to polymer composite deposition AM, especially the large-scale applications.

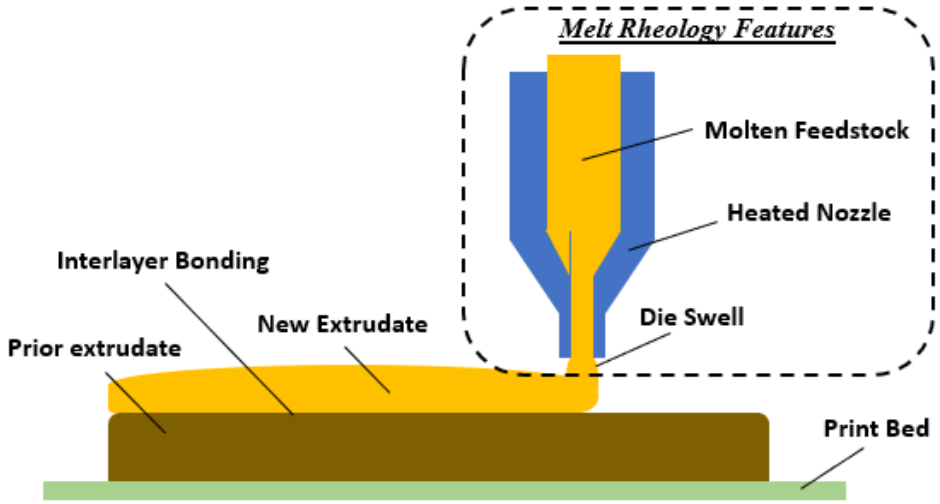

Figure 2. Polymer deposition additive manufacturing diagram. Specific features highlighted by the dash line box are those that influence the rheology properties of the polymer composite melt.

Flow Domain of Interest

We consider the melt flow within and just outside the exit of the extrusion nozzle of a typical LAAM system, where the material rheology of the melt flow exhibits a significant difference when fibers are included. We do not include the turning deposition flow in this study and instead consider only the axial melt flow of the nozzle where the flow domain of interest can be represented as a 2D axisymmetric model, including the flow inside the nozzle and a short strand of free extrudate. As in prior related literature [12-15], an isothermal Stokes flow is assumed for the model and thus the temperature effect, time transient effects, and inertia effects are ignored in the simulation. Heller, et al. [12] (see also [16,17]) showed that the internal geometry of the nozzle has a significant influence on the fiber orientation of the extruded composite, since the flow domain geometry defined by the interior of the nozzle defines the melt flow velocity gradient fields. To eliminate the influence of internal nozzle geometry features on our results, the flow model investigated in this paper is a straight tube as shown in Figure 3. The influence of nozzle geometry on fully-coupled polymer composite melt flow is left for future work.

Using the geometry of a Strangpresse large-scale additive manufacturing Model 19 single

screw extruder nozzle as a reference, the radius of the straight tube that defines our flow domain is set as 0.0625 inch [13]. The ratio of the internal-nozzle length to the radius is 5:1. For simplicity, the length of the free extrudate is set to be equal to the internal-nozzle length of 0.3125 inches.

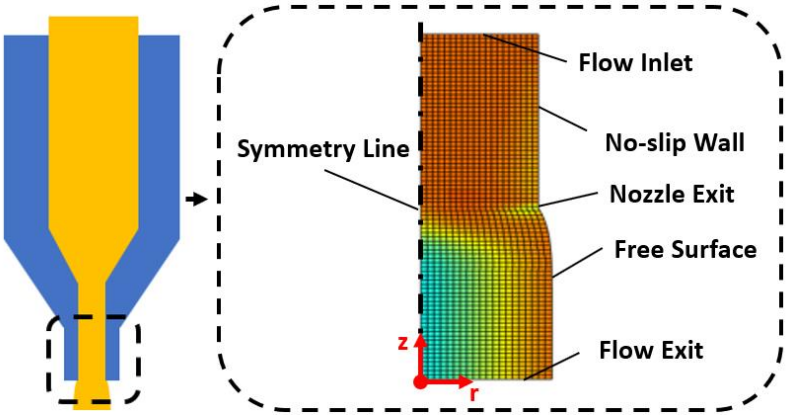

Figure 3. 2D axisymmetric flow domain of interest simplified from an extrusion nozzle geometry.

Governing Equations for Flow and Fiber Orientation

Assuming the polymer melt flow is an isothermal, incompressible, and highly viscous creeping flow, the mass and momentum conservation equations can be written respectively as [18]

$$\nabla \cdot \boldsymbol{v} = 0, \tag{1}$$

and

$$-\nabla p + \nabla \cdot \boldsymbol{\tau} = 0, \tag{2}$$

where $\boldsymbol{v}$ is the velocity vector, p is the melt pressure and $\boldsymbol{\tau}$ is the stress tensor associated with the shear deformation. Equations 1 and 2 neglect the thermal gradients, inertia effects and time-transient effects of the fluid flow, which is assumed to yield little contribution to the fiber-flow coupling properties of LAAM as suggested by [12-15].

Advani and Tucker [10] proposed the widely used tensor approach for modeling fiber orientation within a polymer melt flow. This approach statistically quantifies the fiber orientation kinetics in a flow domain through

$$\frac{\mathrm{D}\boldsymbol{A}}{\mathrm{Dt}} = (\boldsymbol{A}\cdot\boldsymbol{W} - \boldsymbol{W}\cdot\boldsymbol{A}) + \lambda(\boldsymbol{A}\cdot\boldsymbol{D} + \boldsymbol{D}\cdot\boldsymbol{A} - 2\boldsymbol{D}\colon\mathbb{A}) + 2C_I\dot{\gamma}(\boldsymbol{I} - 3\boldsymbol{A}), \tag{3}$$

where the second- and fourth-order fiber orientation tensors are defined respectively as

$$\boldsymbol{A} = A_{ij} = \oint_{\mathbb{S}} s_i s_j \delta(s) d\mathbb{S} \quad \text{and} \quad \mathbb{A} = A_{ijkl} = \oint_{\mathbb{S}} s_i s_j s_k s_l \delta(s) d\mathbb{S}, \tag{4}$$

In the above, the unit vector $\boldsymbol{s}$ defines the direction of a single rigid fiber, and $\delta(s)$ is the fiber orientation probability distribution function for $\boldsymbol{s}$ defined over the surface $\mathbb{S}$ of a unit sphere. It is important to note that due to the normalization condition, the integral of $\delta(s)$ over the surface equates to one, which yields the trace of $\boldsymbol{A}$ to be the unity. In addition, the $\boldsymbol{A}$ tensor is symmetric, which along with the normalization condition, yields five independent variables in the $\boldsymbol{A}$ tensor. In polymer melt flow fiber orientation calculations, the forth order fiber orientation tensor $\mathbb{A}$ is typically expressed as a function of $\boldsymbol{A}$ through a closure approximation (for example, the hybrid closure [19], the natural closure [20], the invariant-based fitted closure [21], and the orthotropic closure

[11]). In this study, we employ the orthotropic fitted closure [11] due to its stable behavior in related literature [12-15]. Notice, the fiber length for short-fiber reinforced thermoplastics in LAAM is typically much smaller than the nozzle diameter. Therefore, we employ continuum mechanics theory for Equation 3 and thus the fiber orientation tensor field is a continuous function of position and time. Here, we use nodal values of the finite element domain to discretize A and then interpolate A over each element with shape functions (c.f. [11] for detail).

Additionally, $\boldsymbol{D}$ and $\boldsymbol{W}$ appearing in Equation 3 are the strain rate tensor and vorticity tensor, respectively, which can be written respectively as

$$\boldsymbol{D} = (\nabla \boldsymbol{v} + \nabla \boldsymbol{v}^T)/2 \text{ and } \boldsymbol{W} = (\nabla \boldsymbol{v} + \nabla \boldsymbol{v}^T)/2, \quad (5)$$

Here, $\nabla \boldsymbol{v}$ indicates the flow deformation gradient field and the superscript T refers to the matrix transpose operation. In addition, $\dot{\gamma}$, λ, and C_I in Equation 3 are, respectively, the scalar magnitude of $\boldsymbol{D}$, a parameter accounting for the effects of fiber hydrodynamic aspect ratio, and an empirical coefficient counting the fiber-fiber interaction effect. Specifically, λ [10] and C_I [22] can be expressed respectively as

$$\lambda = \frac{(a_r)^2 - 1}{(a_r)^2 - 1}, \quad (6)$$

and

$$C_I = 0.0184 \exp(-0.7148 v_f a_r), \quad (7)$$

where a_r is fiber hydrodynamic aspect ratio and v_f refers to the fiber volume fraction. In addition, several literatures cited above (e.g., [10,12-15]) are recommended to readers interested in a systematic review of the fiber orientation kinetics characterization.

Flow-Fiber Coupling

A computationally efficient method to characterize the fiber reinforced composite suspension in polymer processing applications is the flow-fiber one-way weakly coupling formulation (also known as the decoupled scheme), where the flow field is computed ignoring the influence of fiber orientation within the melt flow, and then the fiber orientation tensor field is computed based on the uncoupled flow kinematics results. The decoupled scheme is shown to be sufficiently accurate in shear dominated narrow gap flows such as those common to injection molding [23] and compression molding [24].

Alternatively, Evans, et al. [25] showed that a rigorous simulation of fiber suspension flow should include the effect of the flow on fiber orientation as well as the fiber orientation influence on the polymer melt rheology, which is considered as the “fully-coupled” calculation. Libscomb, et al. [26] conducted experimental and corresponding numerical studies for fiber suspension with a Newtonian solvent and their results including the effects of the flow-fiber coupling effects. Their computed results showed a good agreement with the experimental measurement. Dinh and Armstrong [27] developed a rheological constitutive equation for semi-concentrated and concentrated fiber suspensions in which the effects of fiber aspect ratio, fiber volume fraction, and fiber orientation on the flow-fiber coupling intensity are included. The Dinh-Armstrong model has seen application in polymer composite melt flow calculations [26,28] due to its simplicity and accuracy. Tucker [29] employed a dimensionless particle number N_p to characterize the intrinsic anisotropic effect of the fibers on melt flow rheology in narrow gap flows. In this approach, the stress tensor in Equation 2 is modified to include the effect of fiber orientation on effective viscosity as [29]

$$\boldsymbol{\tau} = 2\eta \boldsymbol{D} + 2\eta N_p \mathbb{A} : \boldsymbol{D}, \tag{8}$$

where η is the isotropic melt viscosity. Based on the micromechanical model in Dinh and Armstrong [27], the particle number N_p appearing in Equation 8 may be written as a function of the fiber volume fraction and fiber aspect ratio as

$$N_p = K v_f / (1 + J v_f), \tag{9}$$

where K and J are coefficients related to the material model applied. Here, K is written as [29]

$$K = \frac{(a_r)^2}{3 ln \sqrt{\pi / v_f}}, \tag{10}$$

The Dinh-Armstrong model is extended from a slender-body theory-based model (e.g., see Batchelor [30]), which assumes that the particle's thickness can be ignored yielding $J = 0$ in Equation 9. The slender-body assumption makes it possible to incorporate fiber-fiber hydrodynamic interactions in an averaged sense, allowing this approach to be applicable beyond the dilute regime [29]. In addition, the expressions for N_p in Equations 9 and 10 are derived by assuming a fully aligned fiber orientation which is supported by weakly coupled studies [12-15] of fiber orientation in LAAM applications. Hence, we apply the fully aligned assumption for defining the N_p.

Finally, polymer melt exhibits strong non-Newtonian flow behavior which is typically modeled for purely viscous fluids as a shear rate dependent viscosity in Equation 8. We employ the power law Generalize Newtonian Fluid model to represent the well-known shear thinning behavior of thermoplastics and short fiber-filled thermoplastics. The viscosity of a power law fluid may be written as [18]

$$\eta(\dot{\gamma}) = M(\dot{\gamma})^{n-1} \tag{11}$$

where M is the consistency index and n is the power-law index.

Polymer Extrudate Free Surface Computation

To consider the influence of fiber orientation on die swell, our fully coupled flow-fiber analysis must also include a free surface extrudate shape computation. The extrudate free surface shape has been computed for fused filament fabrication simulations (e.g., [12-15,31,32]) where Heller, et al. [12,15] developed a custom MATLAB (Natick, MA, USA) program to determine the optimum free surface shape by minimizing the integrated normal stress along element edges that compose the free boundary. The subroutine was in conjunction with the built-in remeshing function of commercial finite element suite COMSOL (Burlington, MA, USA). Alternatively, Tanner, et al. [33] computed the location of the free surface boundary for an axisymmetric flow by considering free surface as a streamline such that the position of successive points along the free surface follows

$$r_{i+1}^{(j)} = r_i^{(j)} + \int_{z_i}^{z_{i+1}} \frac{v_r}{v_z} dz, \tag{12}$$

where r is the radial coordinate of points on the free surface, and z is the direction parallel to the flow (e.g., cylindrical coordinates appearing in Figure 3). We compute the radii of surface nodes with Equation 12 as shown in Figure 4 where the subscript i indicates successive node numbers starting at 0 with r_0 referring to the intersecting node of the no-slip wall and free extrudate surface, which is a fixed node having known coordinate values.

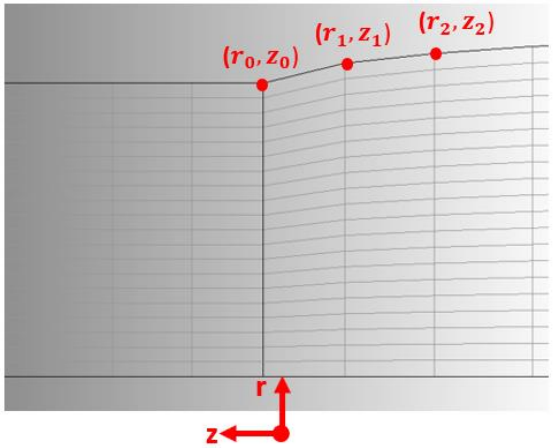

Figure 4. Schematic diagram of the streamline-wise remeshing approach. Note, the domain is rotated 90 degree counterclockwise as compared to Figure 3.

Additionally, the location of the free surface boundary cannot be obtained in a single step but instead requires an iterative scheme where the superscript j refers to the iteration number. We found that four iterations are typically sufficient to yield a converged free surface boundary location for a coarse meshed axial flow [33,34]. Convergence of free surface iterations is assumed based on the die swell ratio of the extrudate, which is written as

$$B^{(j)} = r_n^{(j)}/r_0, \tag{13}$$

where B is the die swell ratio, $r_n^{(j)}$ refers to the radial coordinate of the last node (n-th node) of the free surface along the flow direction at the j-th iteration.

Solution Scheme

VerWeyst and Tucker [11] conducted a melt flow-fiber orientation fully coupled analysis for several internal flow geometries by formulating Equations 1,2,3 and 8 into an integrated finite element scheme through the Galerkin Finite Element Method (GFEM) (e.g., see [35]) using the commercial finite element code, FIDAP. Our approach is similar except that we solve the GFEM-formulated flow and fiber orientation problems with a custom MATLAB code developed for this purpose and include the free surface calculation described above. As seen in [11], the melt flow-fiber orientation coupling simulation seldom converges without special attention to the iteration process (e.g., Newton Raphson method [36], Picard iterative method [37]). Here, we decompose the system into two sub parts: the flow module, which computes a solution to Equations 1, 2, 8, 11 and 12, and the fiber orientation module, where Equation 3 is solved numerically. The algorithm starts by computing the flow field assuming a constant known fiber orientation. Then the extrudate swell ratio of the computed free surface location is evaluated through an iterative solution of Equation 13. for a computed flow field, nodal fiber orientation tensor values are computed using Equation 3 with a time-marching forward Euler method. The time-marching scheme yields the steady state fiber orientation solution upon its convergence (e.g., difference between two successive solutions are within a prespecified small error). After the computation of the fiber orientation, the flow field is updated with the assumed constant fiber orientation results. The iteration between the two sub-modules continues until convergence is achieved. A flowchart illustrating the proposed algorithm is given in Figure 5.

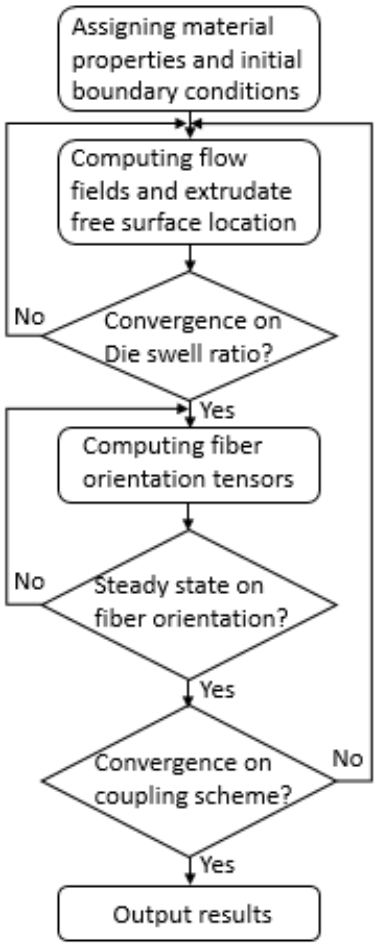

Figure 5. Flowchart of the proposed algorithm.

Computed Results

The algorithm described above is employed to analyze the melt flow-fiber coupling effects on melt extrusion process of LAAM applications. The flow field for various fiber volume fractions and fiber aspect ratios is computed and compared. Furthermore, we evaluate the die swell for each where details of the computed results are given below.

Material Properties and Boundary Conditions

The main focus of this paper is to numerically determine the flow-fiber coupling effects in LAAM applications. Here, we employ the rheology properties of a 13% CF-ABS polymer, which has experienced widespread applications in melt extrusion AM research [1,2,12-15]. After fitting the shear viscosity data of 13% CF-ABS at 215 °C reported by Wang and Smith [38], we obtain power law fluid parameters of M=1.2 × 10^4 (Pa s^n) and n=0.51. Notice, the following simulations are performed over a range of fiber volume fraction and aspect ratio while power law model parameters are assumed constant and not a function of fiber orientation for simplicity and consistency. It is important to note that that the shear viscosity behavior of filled polymer varies due to the fiber volume fraction and fiber aspect ratio(e.g., see [4-7]). Nevertheless, assigning

material properties based on the implemented fiber volume fraction and aspect ratio is still vital when calibrating the printing parameters for a LAAM printing task, which can be a good extension of our presented work.

The flow boundary conditions appear in Figure 3. Specifically, a fully developed velocity profile based on a volume flow rate of $1.2 \times 10^{-6}\ mm^3$ is imposed in the flow inlet. The volumetric flow rate is $1.2 \times 10^{-6}\ mm^3$, which corresponds to a typical LAAM mass flow rate of approximately 9 lb/hour for 13% CF-ABS. In addition, an isotropic fiber orientation field is assumed for the entire flow domain in the first melt flow-fiber orientation iteration, as in VerWeyst and Tucker [11]. Note, Equation 3 for solving the fiber orientation tensors is a hyperbolic format where an initial condition at the inlet of the flow domain is needed. Here, we impose a prescribed the fully developed fiber alignment as reported by Heller, et al. [12].

Flow Fields

Simulations of material melt flow extrusion for LAAM applications have been done under the decoupled flow-fiber framework (e.g., the flow governing equations are solved neglecting the presence of fibers reinforced) by several prior studies [12-15]. With the proposed method, we are able to characterize the mutually dependent effects between the flow and fiber orientation on the velocity fields of the melt. Through Figures 6 and 7, the velocity fields at two major directions of interest are given for applied composite feedstock with different fiber volume fraction. Note, the fiber aspect ratio of the employed materials is fixed at 10. Also, we define the velocity field along the flow direction as v_z, and that perpendicular to the direction of flow is referred as v_r (c.f. Figure 3 for the definition of 2D cylindrical r-z coordinates).

The computed velocity contours indicate that v_r is at least one order of magnitude lower than that of v_z in most of the flow domain, except in the vicinity of the nozzle exit. The dramatical variations of the velocity fields at the nozzle exit are caused by the change in flow boundary conditions, such that the polymer melt is leaving the fixed-wall part of the domain and is enters the free boundary region. Specifically, the radial-direction velocity increases significantly at the nozzle exit corner, where v_r is nearly one order of magnitude higher than that in most of the flow field. In contrast, the variation v_z occurs over the nozzle exit, where values near the free surface boundary increase while the velocity near the center of the nozzle decreases. Ultimately v_z becomes uniform across the radial direction at the end of the entire flow domain. In these simulations, the extrudate experiences a contraction flow along the centerline of the nozzle which is known to have a significant effect on fiber orientation [12,13]. Specifically, by comparing the sub-figures a-c in Figures 6 and 7, it can be seen that increasing the fiber volume fraction weakens the increase in radial-direction flow field at the nozzle exit, while increasing values of v_z in the free extrudate downstream.

(a)

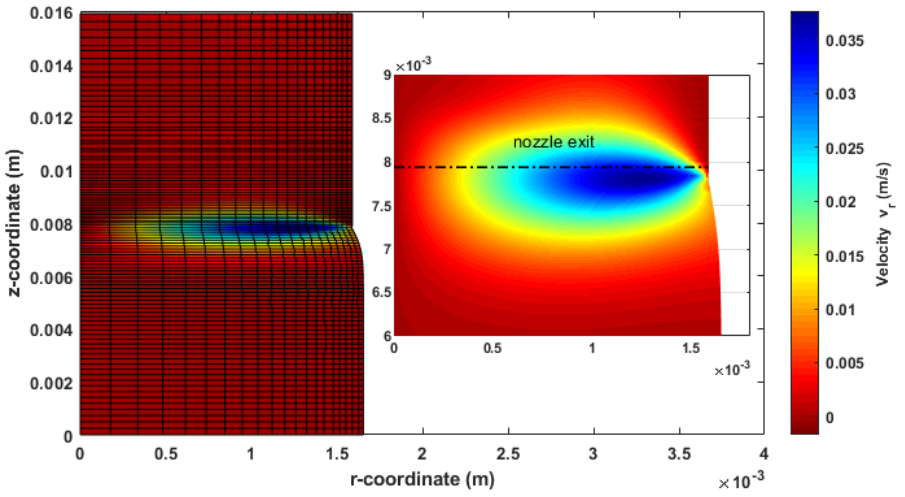

(b)

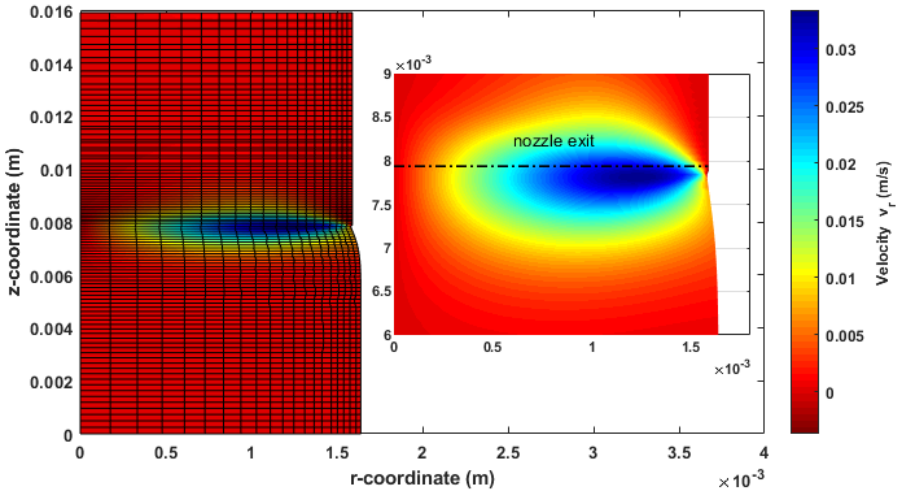

(c)

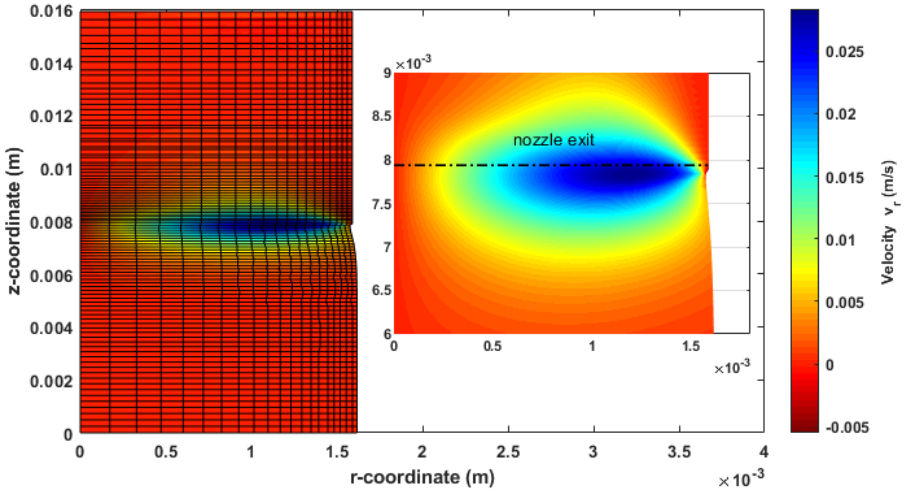

Figure 6. Contours of velocity v_r at different fiber volume faction: (a) v_f=0; (b) v_f=0.12; (c) v_f=0.24. Note, the a_r=10 for the above simulations.

(a)

(b)

(c)

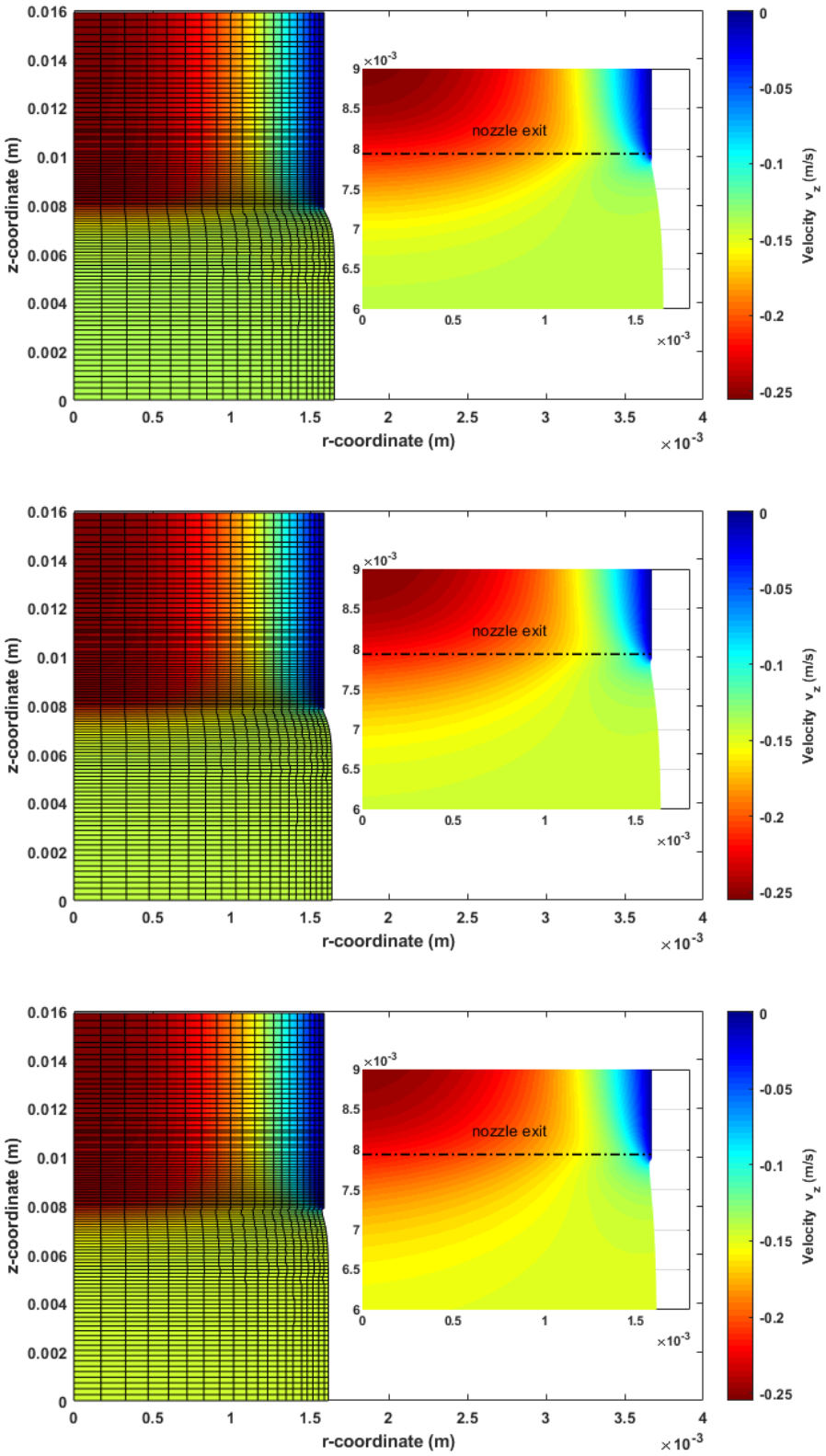

Figure 7. Contours of velocity v_z at different fiber volume faction: (a) v_f=0; (b) v_f=0.12; (c) v_f=0.24. Note, the a_r=10 for the above simulations.

It is important to quantify the effects of fiber loading on the dominant flow field of velocity v_z. 7. The velocity v_z as a function of radial position appears in Figures 8 to 11. Note that radial location appearing in these figures is normalized by nozzle exit radius r_0 where $z/r_0 = 10, 5,$ and 0 refer to the locations of the flow inlet, nozzle exit, and flow exit, respectively (c.f. Figure 3). Specifically, the velocity profiles shown in Figure 8 and 9 indicate that the fully coupled melt flow-orientation computations yield more significant variations as compared to those within the nozzle. In addition, the magnitude of velocity variation increases with the fiber volume fraction. The velocity profiles tend to become more uniform with a value similar to that of the polymer melt near the flow exit. This can be clearly seen as well in the results of v_z profiles across the flow directions appearing in Figures 10 and 11, where the effects of the fiber volume fraction on the flow-direction velocity appear near the nozzle exit as well as in the free extrudate section. It can be seen that adding more fiber content to the polymer feedstock increases the final v_z near the flow exit. Also, the velocity profiles along the flow direction quickly reach a steady state shortly after the melt passes the nozzle exit.

Computed velocities v_z at the flow exit appear in Table I. The increased fluid velocity magnitude along the extrusion direction appears to be a result of shear thinning within the polymer melt as mentioned before (cf. [3-5]) within the high shear region (e.g., the flow domain of interest appearing in Figure 3). Here fiber alignment increases the shear rate which increases shear thinning of the polymer melt which also increases the velocity in the direction of flow. Part of the contribution of our proposed code may be to quantify the difference of the melt flow kinematics due to the addition of fibers and thus the printing conditions of the LAAM machine could be adjusted based on computed information.

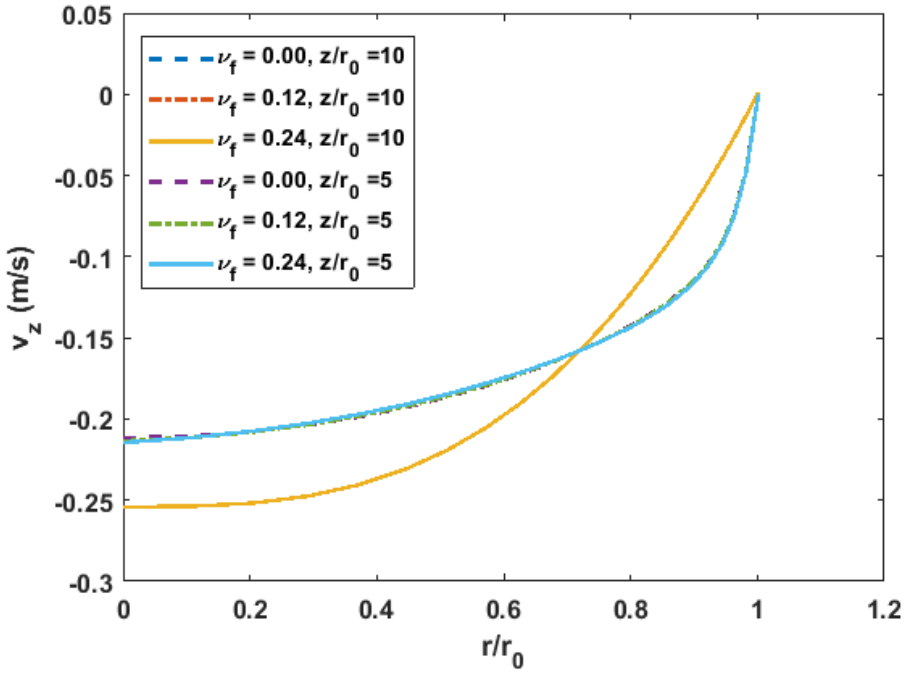

Figure 8. Flow-direction velocity profile (internal nozzle) across radial direction.

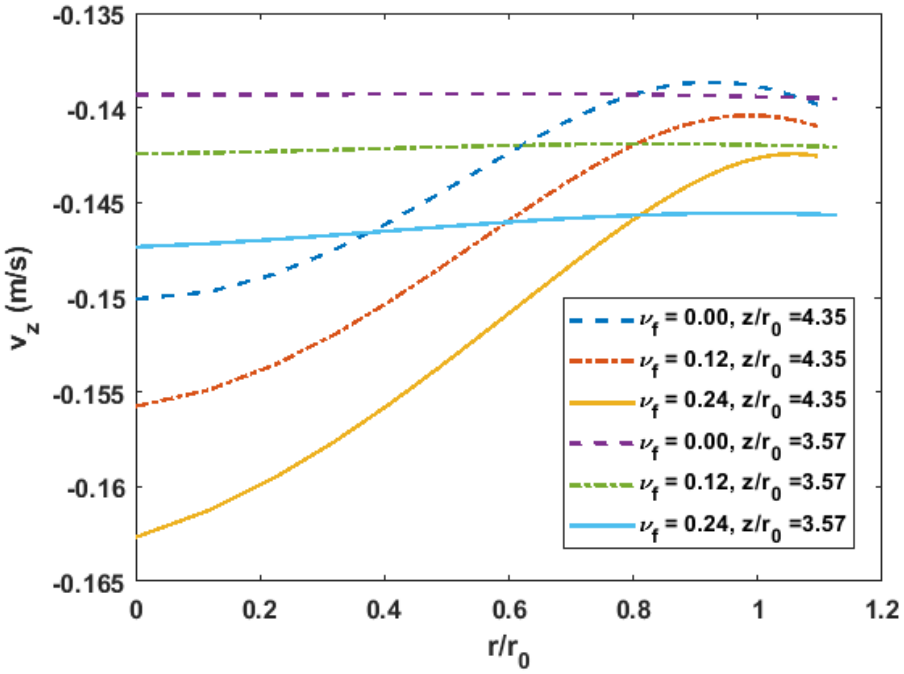

Figure 9. Flow-direction velocity profile (free extrudate) across radial direction.

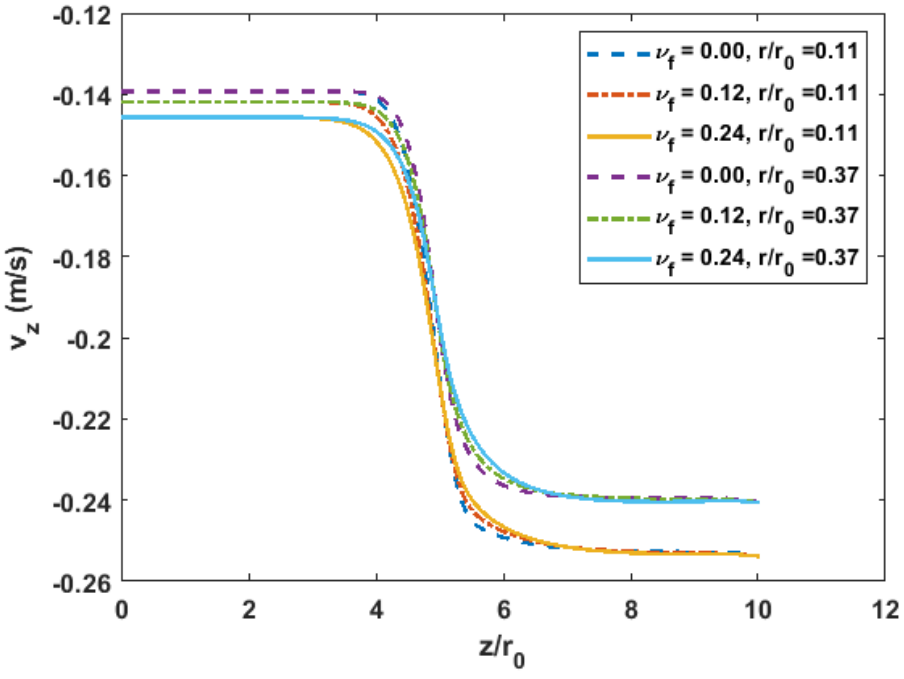

Figure 10. Flow-direction velocity profile (internal nozzle) along direction of extrusion.

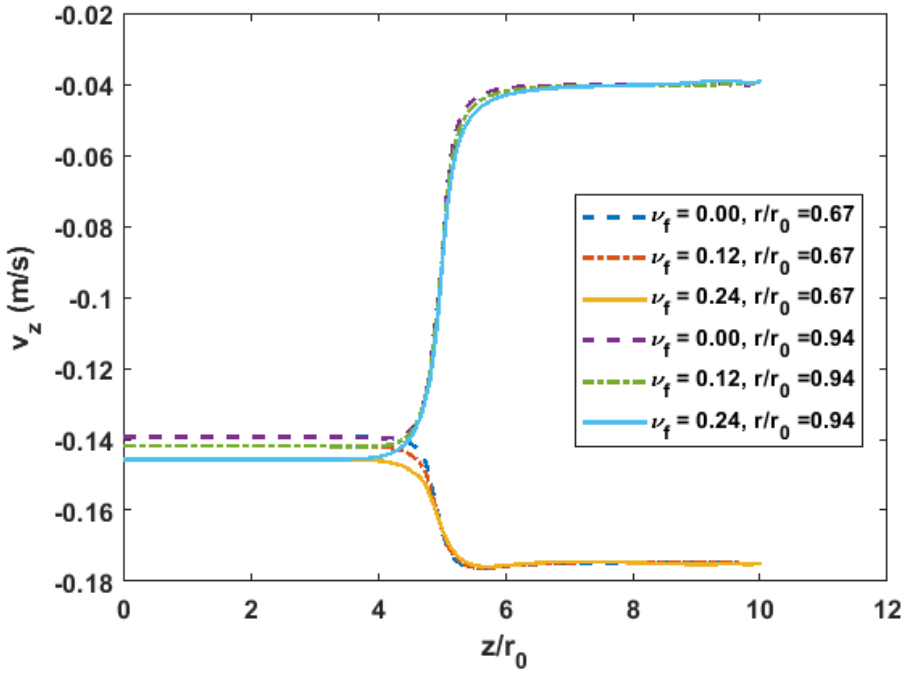

Figure 11. Flow-direction velocity profile (free extrudate) along direction of extrusion.

Table I: Predicted v_z at the Flow Exit with Different Fiber Volume Fraction Applied.

Fiber Volume Fraction	v_z at Flow Outlet (mm/s)	Radius of Flow Exit (mm)
0	139	1.65
0.12	142	1.64
0.24	146	1.62

*Note, the radius of the nozzle exit (c.f. Figure 3) is 1.59 mm.

Extrudate Swell

From computed data appearing in Table I, it can be seen that the radius of the free extrudate at the flow domain exit reduces as the fiber volume fraction increases, a result that is similar to that reported in Hideyuki, et al. [7]. We simulate the extrusion process with different fiber aspect ratio and fiber volume fraction, and quantify the die swell ratio (c.f. Equation 14) of the free extrudate at the flow exit (c.f. Figure 3). Computed die swell ratio for various aspect ratios and volume fractions appear in Figure 12, where fiber aspect ratio of 10, 15, and 20 are considered. It should be noted that increasing the fiber volume fraction yields an increase in the nonlinearity of the coupled system which ultimately makes convergence of the melt flow-fiber orientation iterations difficult. This issue is alleviated somewhat with lower fiber aspect ratio which is reflected in the result appearing in Figure 12, where lower fiber aspect ratio case can simulate higher fiber volume fraction. From the computed data, it is seen that die swell ratio reduces with an increasing fiber volume fraction. Increasing the fiber aspect ratio also decreases the trend of extrudate swell of the melt. Moreover, a nearly linear relationship is seen between the fiber volume fraction and

the die swell ratio. Additionally, the reduction of die swell with increasing fiber aspect ratio exhibits a steeper gradient as compared to that computed by implementing a lower fiber aspect ratio.

Based on results appearing in Figure 12, we fit a linear relationship and the fitted results appear as the dash lines shown in Figure 13. The fitted coefficients of the linear curves appear in Table II. In addition, we also linearly interpolate computed data with different fiber aspect ratio values using the known data at a_r=10,15, and 20 at a given fiber volume fraction through the MATLAB function “spline” [39]. Ultimately, the effect of the fiber aspect ratio and the fiber volume fraction on the resulting die swell ratio is obtained, as given in Figure 14. It is clearly seen that either an increasing fiber volume fraction or increasing fiber aspect ratio leads to a notable reduction in the predicted die swell ratio of the free extrudate. Although the computed die swell ratios are linearly interpolated in both fiber volume fraction and fiber aspect ratio, it is found that the resulting fitted curves are not uniformly distributed. Thus, we further compute the gradient of the die swell ratio field with respect to the fiber volume fraction and aspect ratio, where the results appear in Figures 15 and 16. It can be seen that the trend of predicted die swell ratio more closely follows the gradient field with respect to the fiber aspect ratio rather than that of fiber volume fraction. These results show that the effect of fiber volume fraction on the resulting die swell ratio is linearly increases regardless of the fiber aspect ratio, while the impact of the fiber aspect ratio is enhanced with an increased fiber volume fraction.

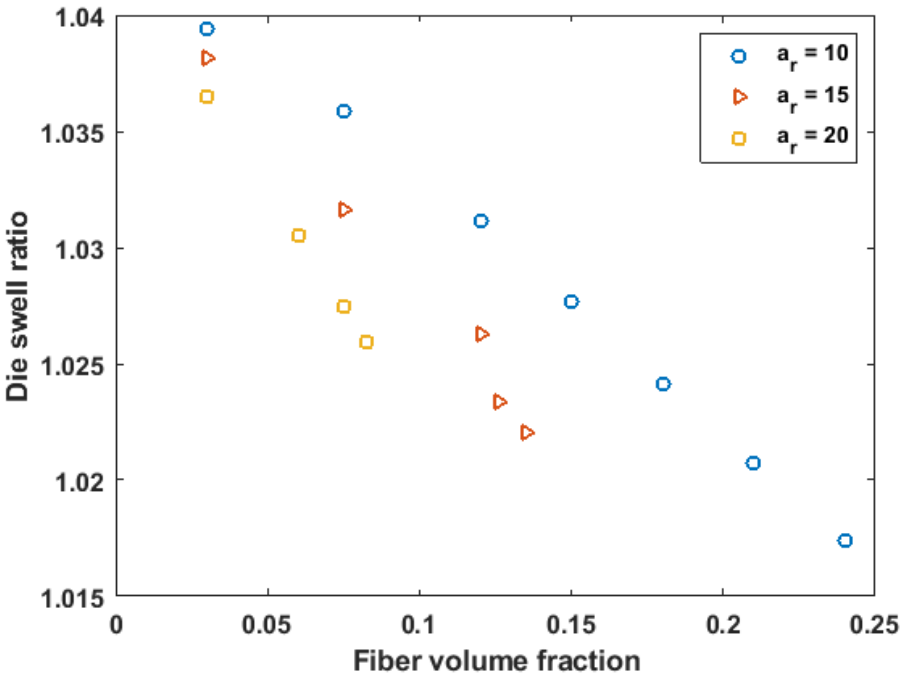

Figure 12. Predicted die swell ratio at flow outlet with different parameters applied.

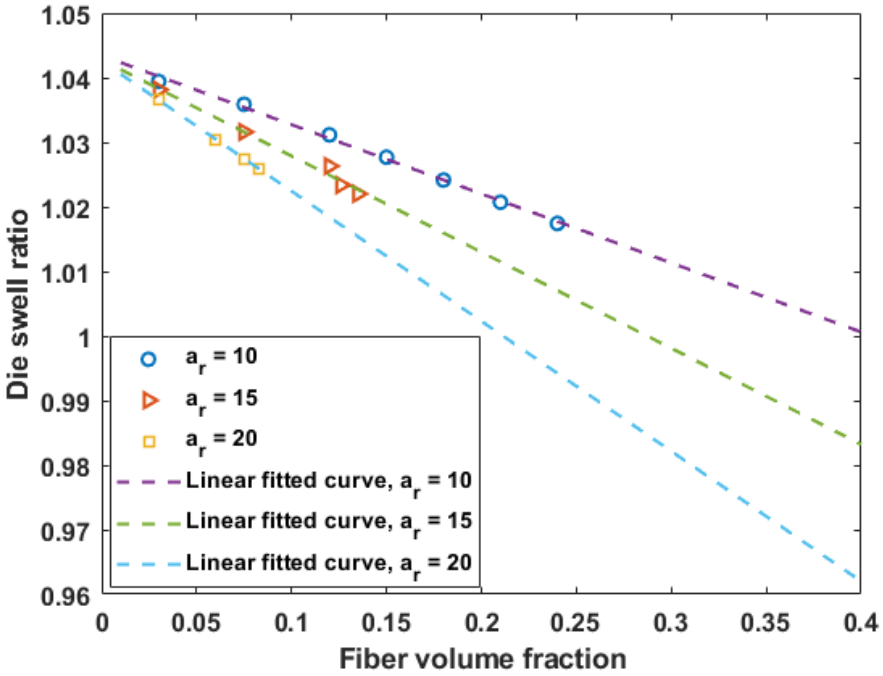

Figure 13. Linear curve fitting of the predicted die swell ratio data.

Table II: Linear Fitted Coefficients of Curves Appearing in Figure 13.

Fiber Aspect Ratio	Fitted Slope	Linear Constant
10	-0.1070	1.0434
15	-0.1488	1.0428
20	-0.2014	1.0426

*Note, the fitted slope ($\hat{k}$) and linear constant ($\hat{b}$) are coefficients of a linear fitted curve, such that $B = \hat{k} \times a_r + \hat{b}$.

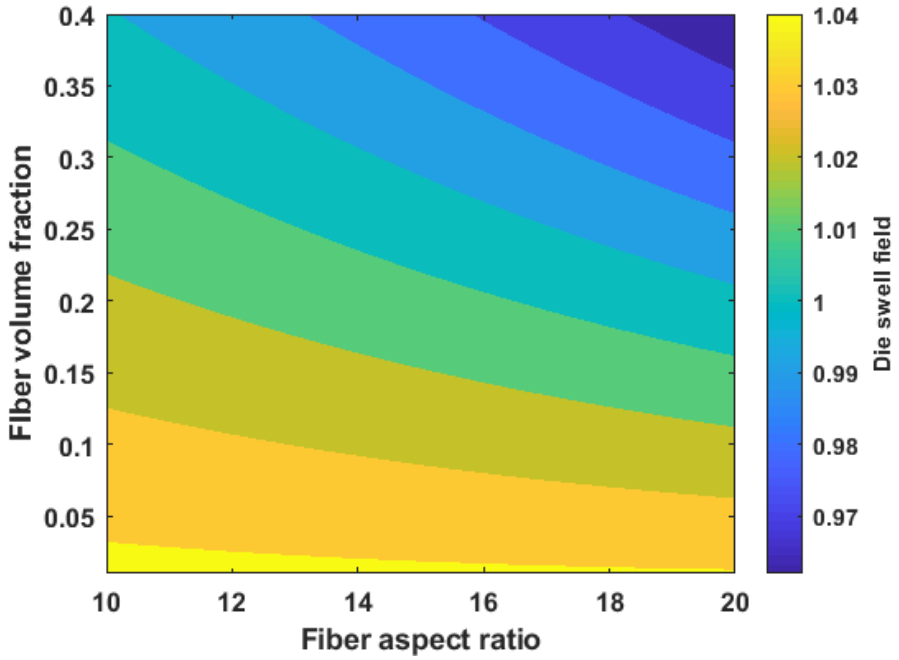

Figure 14. Predicted die swell ratio field of filled polymer at different fiber volume fraction and fiber aspect ratio.

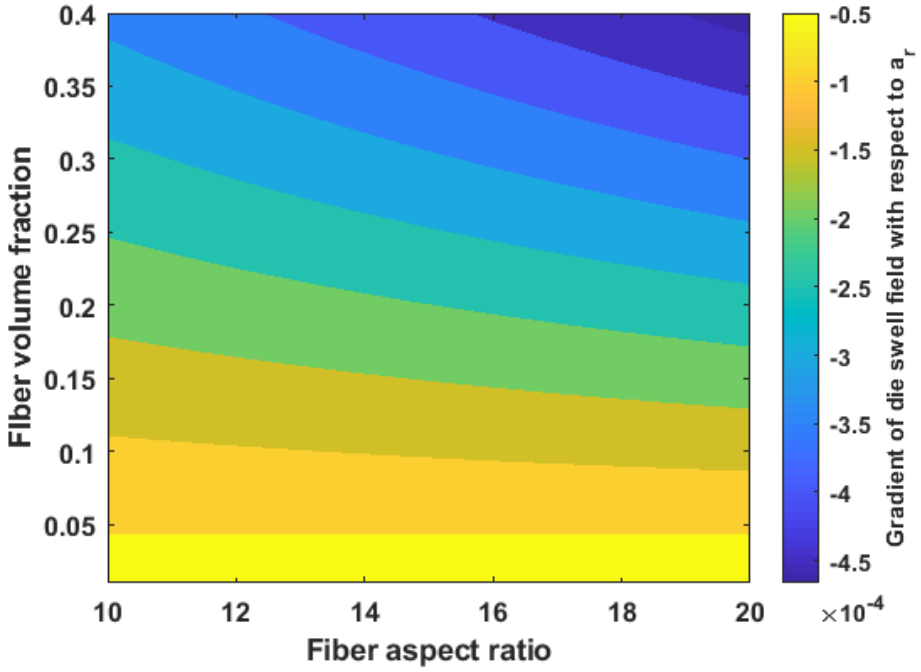

Figure 15. Gradient field of the predicted die swell ratio field with respect to a_r.

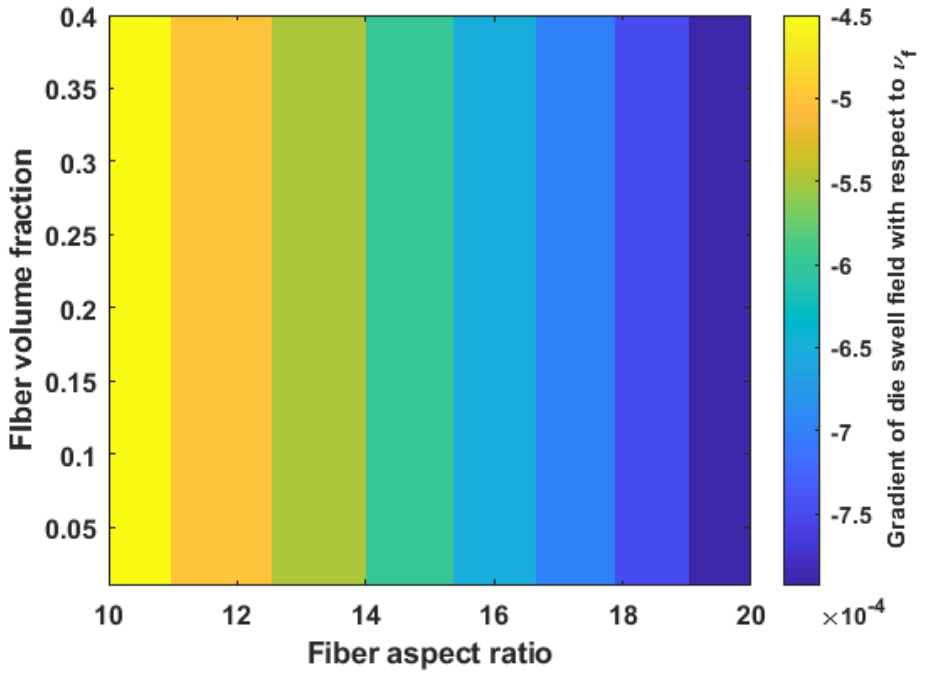

Figure 16. Gradient field of the predicted die swell ratio field with respect to υ_f.

Discussion

Compared to traditional FFF, the unique screw extrusion mechanism of LAAM systems enables a larger selection of polymer and polymer composite materials [2]. Unfortunately, to date, the process-structure-property relations for polymer composite deposition is still unclear and long trial-and-error discovery process is needed for using a specific polymer composite in LAAM applications. Extrudate melt flow simulations such as those presented above may benefit large-scale AM technology as follows:

- Calibration of material feeding rate

  The material feed rate and material deposition rate including the effects of die swell must be coordinated, otherwise the deposited bead may be blocked at the nozzle exit or disconnected on the substrate (c.f. Figure 17). In addition, our proposed algorithm also demonstrates the influences of fiber volume fraction and fiber aspect ratio on the flow fields of melt flow extrusion. This is particularly useful as the volume fraction and aspect ratio (in average) of the composite feedstock could be measured in advance.

- Adjustment on printing raster

  Extrudate swell of the molten polymer affects the resolution of a printed part, especially in the case of a LAAM application. Using a same printing raster, we print two samples using the neat ABS polymer and 13% CF-ABS, separately. Some detail of the printed samples is given in Figure 18, where delamination (e.g., appearing in A-2) and voids (e.g., appearing in B-2) are clearly seen in the structure printed using CF-ABS. This is a result of the changing geometry of deposited beads of filled ABS as compared to the virgin polymer. Although the geometry of a lay-down bead and a vertical extrudate are different, our computed results (c.f. Figure 12)

can provide some referential information in adjusting the printing raster in order to compensate the geometrical variation of the polymer composite extrudate due to the addition of the fiber fillers.

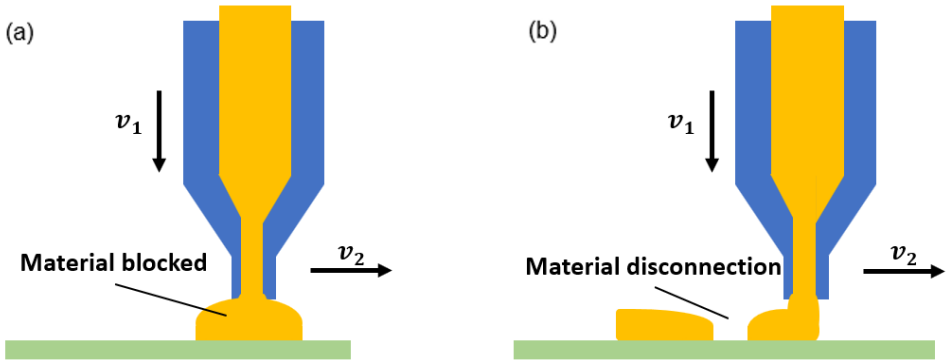

Figure 17. Printing failures occurred due to the un-equilibrium of material feeding rate (v_1) and deposition rate (v_2): (a) material blocked when $v_1 \gg v_2$; (b) material disconnected when $v_1 \ll v_2$.

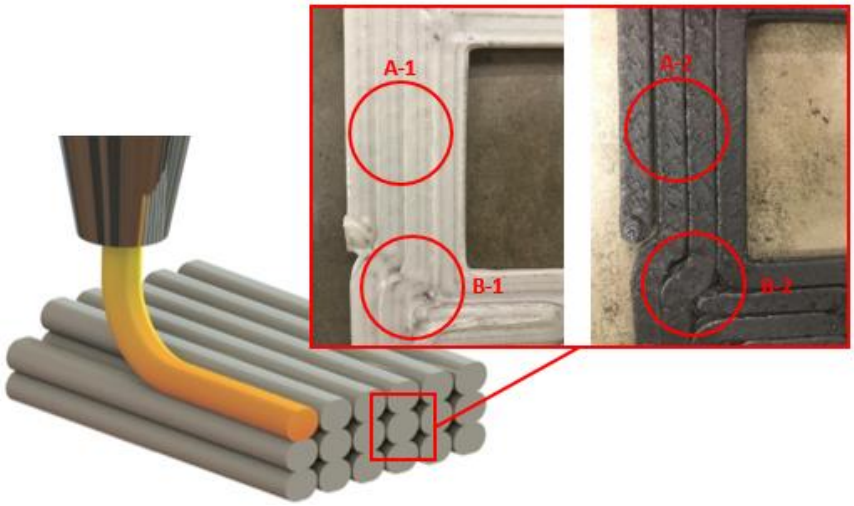

Figure 18. Effects of extrudate swell on the resolution of a printed part. Note the white sample is printed with neat ABS polymer and the black one is made with 13% CF-ABS.

Summary and Next Steps

This study numerically simulates the effects of flow-fiber orientation coupling on the flow kinematics and melt extrudate swell for a Large Area Additive Manufacturing (LAAM) polymer composite deposition process. The mutually dependent impacts between the polymer flow and the fiber orientation kinetics are quantified through a two-way fully coupled iterative scheme developed using the Galerkin Finite Element Method (GFEM), where the non-Newtonian shear thinning behavior of the polymer melt viscosity is included and the effect of fiber orientation distribution on the flow enters the problem through an effective anisotropic viscosity.

The computed results show that the presence of fibers and their orientation pattern yield a significant impact on the flow field kinematics of the polymer melt during the melt extrusion process, especially within the free extrudate. Specifically, the magnitude of the velocity profile along the flow direction increases with an increasing fiber volume fraction. In addition, the trend of the melt extrudate swell reduces with fibers loaded into the feedstock. By either increasing the fiber volume fraction and/or fiber aspect ratio, the die swell ratio of the free extrudate reduces by a notable amount.

For the future work, we suggest incorporating our numerical findings to the calibrations of a LAAM machine printing parameters, thus avoiding otherwise the tedious trial-and-error empirical testing process for applying a specific polymer composite feedstock to LAAM applications. In particular, the flow fields information can be used as a refence in calibrating the equilibrium between the material feeding rate and deposition rate. The computed die swell ratio of a vertical extrudate may provide some reference in adjusting the printing raster to compensate the geometrical change of the printed bead.

Acknowledgements

The authors would like to thank as the financial support from Department of Mechanical Engineering at Baylor University. We would also like to thank the Strangpresse Corporation donating their Model-19 extruder that enables us to build up a LAAM system for learning the material deposition process. We also appreciate the help from Mr. Timothy Russell from Baylor University for the preliminary tests of the LAAM system and the many beneficial fiber orientation discussions with Dr. David Jack at Baylor University.

Bibliography

1. Post, Brian K., et al. THE DURABILITY OF LARGE-SCALE ADDITIVE MANUFACTURING COMPOSITE MOLDS. Oak Ridge National Lab.(ORNL), Oak Ridge, TN (United States). Manufacturing Demonstration Facility (MDF), 2016.
2. Duty, Chad E., et al. "Structure and mechanical behavior of Big Area Additive Manufacturing (BAAM) materials." Rapid Prototyping Journal 23.1 (2017): 181-189.
3. Tekinalp, Halil L., et al. "Highly oriented carbon fiber–polymer composites via additive manufacturing." Composites Science and Technology 105 (2014): 144-150.
4. Jain, Sachin, et al. "Strong decrease in viscosity of nanoparticle-filled polymer melts through selective adsorption." Soft Matter 4.9 (2008): 1848-1854.
5. Nikzad, Mostafa, et al. "Rheological properties of a particulate-filled polymeric composite through fused deposition process." Materials Science Forum. Vol. 654. Trans Tech Publications, 2010.
6. Joseph, P. V., et al. "Effect of processing variables on the mechanical properties of sisal-fiber-reinforced polypropylene composites." Composites science and Technology 59.11 (1999): 1625-1640.
7. Hideyuk, et al. "Origin of Reduction in Extrudate Swell of Molten Polymer by Adding of Rigid Fillers." Journal of Textile Engineering 64.4 (2018).
8. Guo, Rong, et al. "Rheology of fiber filled polymer melts: Role of fiber‐fiber interactions and polymer‐fiber coupling." Polymer Engineering & Science 45.3 (2005): 385-399.
9. Ajinjeru, Christine, et al. "The influence of dynamic rheological properties on carbon fiber-reinforced polyetherimide for large-scale extrusion-based additive manufacturing." The International Journal

of Advanced Manufacturing Technology 99.1-4 (2018): 411-418.

10. S. G. Advani and C. L. Tucker III, “The use of tensors to describe and predict fiber orientation in short fiber composites,” J. Rheol., vol. 31, no. 8, pp. 751–784, 1987.
11. VerWeyst, Brent E., and Charles L. Tucker III. "Fiber suspensions in complex geometries: Flow/orientation coupling." The Canadian Journal of Chemical Engineering 80.6 (2002): 1093-1106.
12. B. P. Heller, D. E. Smith, and D. A. Jack, “Effects of extrudate swell and nozzle geometry on fiber orientation in Fused Filament Fabrication nozzle flow,” Addit. Manuf., vol. 12, pp. 252–264, Oct. 2016.
13. Z. Wang and D. E. Smith, “Rheology Effects on Predicted Fiber Orientation and Elastic Properties in Large Scale Polymer Composite Additive Manufacturing,” J. Compos. Sci., vol. 2, no. 1, p. 10, 2018.
14. T. Russell, B. Heller, D. A. Jack, and D. E. Smith, “Prediction of the Fiber Orientation State and the Resulting Structural and Thermal Properties of Fiber Reinforced Additive Manufactured Composites Fabricated Using the Big Area Additive Manufacturing Process,” J. Compos. Sci., vol. 2, no. 2, p. 26, 2018.
15. Heller, Blake P., Douglas E. Smith, and David A. Jack. "Planar deposition flow modeling of fiber filled composites in large area additive manufacturing." Additive Manufacturing 25 (2019): 227-238.
16. J. Nixon, B. Dryer, D. Chiu, I. Lempert, and D. I. Bigio, “Three parameter analysis of fiber orientation in fused deposition modeling geometries,” Annu. Tech. Conf. - ANTEC Conf. Proc., vol. 2, pp. 985–995, Jan. 2014.
17. Garcia, Adrian. Nozzle geometry effects on exit orientation of short fiber composites. Diss. Wichita State University, 2017.
18. Baird, Donald G., and Dimitris I. Collias. Polymer processing: principles and design. John Wiley & Sons, 2014.
19. S. G. Advani and C. L. Tucker III, “Closure approximations for three-dimensional structure tensors,” J. Rheol., vol. 34, no. 3, pp. 367–386, 1990.
20. H. H. De Frahan, V. Verleye, F. Dupret, and M. J. Crochet, “Numerical prediction of fiber orientation in injection molding,” Polym. Eng. Sci., vol. 32, no. 4, pp. 254–266, 1992.
21. D. H. Chung and T. H. Kwon, “Fiber orientation in the processing of polymer composites,” Korea-Aust. Rheol. J., vol. 14, no. 4, pp. 175–188, 2002.
22. R.S. Bay, Fiber Orientation in Injection Molded Composites: A Comparison of Theory and Experiment, Ph.D. Thesis University of Illinois Urbana-Champaign, 1991.
23. Bay, Randy S., and Charles L. Tucker III. "Fiber orientation in simple injection moldings. Part I: Theory and numerical methods." Polymer composites 13.4 (1992): 317-331.
24. Advani, Suresh G., and Charles L. Tucker III. "A numerical simulation of short fiber orientation in compression molding." Polymer composites 11.3 (1990): 164-173.
25. Evans, J. G. The effect of non-Newtonian properties of a suspension of rod-like particles on flow fields. Theor. Rheol. Halstead Press N. Y. 1975, 224–232.
26. Lipscomb, G. G.; Denn, M. M.; Hur, D. U.; Boger, D. V. The flow of fiber suspensions in complex geometries. J. Non-Newton. Fluid Mech. 1988, 26, 297–325.
27. Dinh, Steven M., and Robert C. Armstrong. "A rheological equation of state for semiconcentrated fiber suspensions." Journal of Rheology 28.3 (1984): 207-227.
28. Ranganathan, Sridhar, and Suresh G. Advani. "A Coupled Solution for the Fiber Orientation and Rheology of Non–Dilute Short Fiber Suspensions in Radial Flow." Theoretical and Applied Rheology. Elsevier, 1992. 874-876.

29. Tucker, C. L. Flow regimes for fiber suspensions in narrow gaps. J. Non-Newton. Fluid Mech. 1991, 39, 239–268.
30. Batchelor, G. K. (1971). The stress generated in a non-dilute suspension of elongated particles by pure straining motion. Journal of Fluid Mechanics, 46(4), 813-829.
31. Bellini, William J., and Rita F. Helfand. "The challenges and strategies for laboratory diagnosis of measles in an international setting." Journal of infectious diseases 187.Supplement 1 (2003): S283-S290.
32. Watanabe, Narumi. Computational and experimental investigation of reinforced polymers for material extrusion additive manufacturing. Diss. Georgia Institute of Technology, 2016.
33. Tanner, R. I., Nickell, R. E., & Bilger, R. W. (1975). Finite element methods for the solution of some incompressible non-Newtonian fluid mechanics problems with free surfaces. Computer Methods in Applied Mechanics and Engineering, 6(2), 155-174.
34. Crochet, M. J., and Roland Keunings. "Die swell of a Maxwell fluid: numerical prediction." Journal of Non-Newtonian Fluid Mechanics 7.2-3 (1980): 199-212.
35. Reddy, J. N. (1993). An introduction to the finite element method. New York.
36. Ben-Israel, A. (1966). A Newton-Raphson method for the solution of systems of equations. Journal of Mathematical analysis and applications, 15(2), 243-252.
37. Rhoades, B. E. (1976). Comments on two fixed point iteration methods. Journal of Mathematical Analysis and Applications, 56(3), 741-750.
38. Wang, Z., and D. E. Smith. "Screw Swirling Effects on Fiber Orientation Distribution in Large-Scale Polymer Composite Additive Manufacturing." Proceedings of the Solid Freeform Fabrication Symposium, Austin, TX, USA. 2018.
39. MATLAB and Statistics Toolbox Release 2018a, The MathWorks, Inc., Natick, Massachusetts, United States.